SCIEPublish

Article

Quorum Sensing Systems Engineering for Enhanced *iso*-Butylamine Production in *Escherichia coli*

Mingxiong Liu [1], Yang Li [1], Pingru Yu [1], Hongxin Fu [1,2,3,*] and Jufang Wang [1,2,3,*]

[1] School of Biology and Biological Engineering, South China University of Technology, Guangzhou 510006, China; 1787858593@qq.com (M.L.); 1239098031@qq.com (Y.L.); 34215251@qq.com (P.Y.)

[2] Guangdong Provincial Key Laboratory of Fermentation and Enzyme Engineering, South China University of Technology, Guangzhou 510006, China

[3] State Key Laboratory of Pulp and Paper Engineering, South China University of Technology, Guangzhou 5100640, China

* Corresponding author. E-mail: hongxinfu@scut.edu.cn (H.F.); jufwang@scut.edu.cn (J.W.)

Received: 2 April 2025; Accepted: 13 May 2025; Available online: 19 May 2025

ABSTRACT: Quorum sensing (QS), characterized by pathway-independence and autonomous control, has been applied in bio-manufacturing, while the lack of versatile and functional regulatory components limits its broader applications. To address this issue, a series of efficient QS systems with diverse properties were established in *Escherichia coli*. Firstly, combinatorial optimization, including element selection and promoter replacement, led to an improvement of 8.82- and 3.03-fold in output range and response threshold, respectively. Then, a library of LuxR mutants was constructed for screening novel variants with decreased sensitivity to acyl-homoserine lactone through the high-throughput screening technique. Notably, the optimal variant V36E/H89L/P97L exhibited a decrease of 266-fold in the sensitivity. As a proof-of-concept, *iso*-butylamine biosynthesis was tested by re-directing pyruvate catabolism using QS circuits, and in particular, a total of 15.4 g/L *iso*-butylamine was generated in strain IB21 during the fed-batch culture, marking a 2.96-fold increase over the static control. Finally, the generated bioproduct reached 44.23 g/L in a bioreactor, representing the highest reported titer so far. In summary, this study not only enriches the genetic toolbox of QS systems, but also facilitates industrial applications in value-added chemical production.

Keywords: Quorum sensing; Regulatory elements; Signal sensitivity; Synthetic biology; *iso*-Butylamine; *Escherichia coli*

1. Introduction

Bio-manufacturing powered by microbial cell factories provides an economical and sustainable approach for producing biomaterials, bulk chemicals, biofuels, and medicines [1]. In particular, traditional static control has been applied in the production of value-added bio-chemicals, such as alcohol [2], alkane [3], and resveratrol [4]. These strategies often cause metabolic burden and disrupt metabolic homeostasis, thereby leading to intermediate accumulation, redox imbalance, and growth retardation [5]. Alternatively, dynamic regulation offers a potential choice for adapting to varying environments by autonomously transforming metabolic modes [6]. For instance, the improved growth promoted a high-level production of shikimate (103.3 g/L) by using an osmotic stress-responsive promoter [7]. On the whole, dynamic control is classified into the cellular, intracellular, and extracellular levels according to the specific signals, of which quorum sensing (QS) is a promising and pathway-independent tool by responding to acyl-homoserine lactone (AHL), autoinducing peptide (AIP), or autoinducer-2 (AI-2) [8,9].

Assisted by a handful of synthetic biology toolkits, great efforts have been made in establishing high-performance QS circuits, which contribute to redirecting metabolic pathways, optimizing metabolic flux, and controlling microbial consortia. Importantly, QS circuits enable autonomous regulation without external inducers, thus increasing market competition [10]. To date, titers of several bioproducts have been enhanced by fine-tuning metabolic flux and reprogramming metabolic network mediated by QS circuits, such as 1,4-butanediol [11], medium-chain fatty acids [12], and validamycin [13]. For instance, pyruvate carboxylase was controlled by a *lux*-type QS circuit, and the altered carbon distribution between the tricarboxylic acid (TCA) cycle and L-threonine pathway led to a 26% increase in engineered

https://doi.org/10.70322/sbe.2025.10008

E. coli [14]. To achieve the simultaneous up- and down-regulation, its function was expanded, and synergetic optimization between the TCA cycle and polyhydroxybutyrate synthesis achieved an improvement of 6-fold compared with static control [15]. Subsequently, QS circuits-derived logic gates achieved the control of complicated pathways by integrating with other regulatory tools [16]. In one case, efficient synthesis of D-glucaric acid competes with the glycolysis pathway [17]. Therefore, the combination of an engineered *myo*-inositol (MI) biosensor with the *esa*-type QS orthogonally down-regulated the glycolysis pathway for accumulating MI, leading to a 4-fold increase in product titer. Apart from pathway optimization, QS circuit enables harnessing population composition for facilitating efficient synthesis and substrate utilization [18,19]. Overall, QS circuits are recognized as a powerful tool for enhancing bioproduction and facilitating the design of complex biosystems.

To achieve precise regulation in different circumstances, the performance of QS circuits requires further optimization [20]. To date, the engineering of QS circuits primarily focuses on combinatorial expression optimization and modification of regulatory elements. On one hand, different promoters or RBSs are attempted to optimize the sensory module. By modulating autoinducer synthase, the varying autoinducer productivity generates diverse response thresholds, thus influencing interaction kinetics between the autoinducers and regulatory proteins. For example, the dynamic range increased 23-fold by magnifying *luxI*/*luxR* expression with constitutive promoters. In the meantime, bisabolene titer was increased by up to 5-fold compared to the original [21]. In addition, element redesign and directed evolution facilitate the acquisition of functionally diverse genetic components. So far, more efforts have centered on the well-studied AHL-based QS systems. Although other QS systems have been identified, non-AHL types (such as AI-2-mediated or AIP-mediated QS) are less amenable to modification due to the requirement for the additional elements [22]. On the other hand, modifying the promoter P_{lux} and refactoring transcriptional factor offer an alternative approach to expand QS toolkit via random mutation, directed evolution or rational engineering [23,24]. For instance, computational simulations proved that variant I46F significantly enhanced the affinity between LuxR and 3-oxooctanoyl-homoserine lactone (3OC6HSL), enabling pathogen detection application in a whole-cell sensor [25]. In general, bioproduct synthesis typically initiates after sufficient biomass accumulation. Nevertheless, the research on modifying LuxR remains limited so far, and it is urgent to expand the QS circuit toolkits to meet diverse requirements by engineering regulatory elements.

In this study, we aimed to establish high-performance QS circuits by screening regulatory elements in *E. coli*. First, a series of QS circuits with diverse dynamic properties was designed based on *lux*-type QS system derived from *Vibrio fischeri*. In particular, the expression of *luxI* and *luxR* was combinatorially optimized for adjusting dynamic range and response threshold. Then, a library of LuxR mutants was constructed for identifying new mutation sites that reduced AHLs affinity for LuxR, thereby expanding the functional diversity of QS circuits. As a proof-of-concept, *iso*-butylamine biosynthesis was tested, which showed the effectiveness and superiority of artificial QS circuits in metabolic control. This work provides valuable insights and a practical framework for designing efficient QS systems in synthetic biology applications.

2. Materials and Methods

2.1. Culture Medium and Chemicals

Luria-Bertani (LB) medium was used for plasmids propagation and circuits analysis, containing 5 g/L yeast extract, 10 g/L tryptone, and 10 g/L NaCl. NM2 medium was used for *iso*-butylamine synthesis, consisting of 40 g/L glucose, 12.5 g/L $(NH_4)_2SO_4$, 4.0 g/L KH_2PO_4, 2.0 g/L $MgSO_4 \cdot 7H_2O$, 4 g/L yeast extract, 0.262 g/L L-isoleucine, 0.262 g/L L-leucine, and 5 mL/L trace metal solution (including 10 g/L $FeSO_4 \cdot 7H_2O$, 2 g/L $CaCl_2$, 2.2 g/L $ZnSO_4 \cdot 7H_2O$, 0.5 g/L $MnSO_4 \cdot 4H_2O$, 1 g/L $CuSO_4 \cdot 5H_2O$, 0.1 g/L $(NH_4)_6Mo_7O_{24} \cdot 4H_2O$, and 0.02 g/L $Na_2B_4O_7 \cdot 10H_2O$, dissolved in 0.5 M HCl). A final concentration of 33 μg/mL chloramphenicol or 100 μg/mL ampicillin was added to sustain the corresponding plasmid. In addition, 100 μg/mL β-D-1-thiogalactopyranoside (IPTG) or a desired concentration of 3OC6HSL was supplemented as the inducer when necessary. 3OC6HSL, *o*-phthaldialdehyde, β-mercaptoethanol, and *iso*-butylamine standard were purchased from Macklin (Shanghai, China). Pyruvate was obtained from Aladdin (Shanghai, China).

2.2. Strains and Plasmids

Strains, plasmids, and primers used in this study are listed in Tables S1–S3. The sequences of heterologous genes employed in this study are showed in Table S4. *E. coli* DH5α was used for plasmid construction, and *E. coli* MG1655 served as the host for QS circuit analysis and bioproduct synthesis. Plasmids pTrcHisA and pBAD33 served as the

backbones for the recombinant plasmid construction.

As for the construction of QS circuit, the pair of genes *luxI/luxR* from *V. fischeri* ES114 were codon-optimized and synthesized at Genewiz (Suzhou, China). Genes *luxI/luxR* from *V. fischeri* JM11 and *lux* promoter were amplified from plasmid pTD103*luxI_sfGFP* [26]. The inducible promoter P_{trc} of pTrcHisA was substituted by the constitutive promoter P_{T5}, P_{LS} or P_{J23118}, and then genes *luxI/luxR* were assembled to form sensor modules. In addition, the L-arabinose-inducible promoter P_{araBAD} of pBAD33 was replaced by promoter P_{lux}, followed by the red fluorescent protein gene *mcherry*, forming a response module.

In the synthesis of *iso*-butylamine, inducible promoter P_{trc} was substituted by promoter P_{luxI} or P_{J23119} to construct plasmids pIBQS, pIB02, and pIB03, with plasmid pIB01 stocked in our laboratory as the skeleton. These plasmids were transformed to yield a series of engineered strains using an electroporator (Eppendorf, Hamburg, Germany).

2.3. Fluorescence Characterization

For characterization analysis of QS circuit, a single colony was inoculated into 50 mL of LB medium for 10 h at 37 ℃. Then, 500 μL of seed culture was transferred into 50 mL fresh LB medium for the analysis at 30 ℃ or 37 ℃. Time-course curve was measured at an interval of 1 or 2 h. Additionally, the samples were taken after 30 h for dynamic range evaluation. The culture was diluted as needed, and 200 μL of diluted samples were transferred into a 96-well plate for measurement by a Multi-detection Microplate Reader (BioTek, Winooski, VT, USA). Cell density was measured by detecting the absorbance at the wavelength of 600 nm (OD_{600}), and mCherry fluorescence intensity was detected by an excitation and emission wavelength of 570 nm and 610 nm, respectively. All fluorescence was normalized with an OD_{600}.

2.4. Construction and Screening of LuxR Mutant Library

To construct a library of LuxR mutants, the error-prone PCR was conducted by *Taq* DNA polymerase (Sangon, Shanghai, China), with the mutation rate enhanced by adding 0.5 mM of $MnCl_2$ and 1.5 mM of $MgCl_2$. The fragments of the plasmid backbone and autoinducer-domain were amplified from plasmid pLuxR, which was generated by deleting *luxI* on plasmid pSM10. Then, the reaction solution was transformed into the host. The mutant library was screened using a two-stage "ON/OFF" screening process by adding exogenous 3OC6HSL. In the "OFF" screening, the mutants grown on LB plate were picked into 700 μL LB medium supplemented with 100 nM of 3OC6HSL for 12 h at 37 °C, and an OD_{600} and mCherry fluorescence were measured by using a Multi-Detection Microplate Reader (BioTek, Winooski, VT, USA). Subsequently, the "ON" screening was performed for the non-luminescent candidates by supplementing with a concentration of 100 nM or 10,000 nM 3OC6HSL for 12 h at 37 ℃. In particular, those candidates with a significant increase in fluorescence intensity at 10,000 nM 3OC6HSL were sequenced for the analysis.

2.5. Microbial Synthesis of iso-Butylamine in Shaking Flasks

A single colony grown on LB plate was inoculated into 50 mL of LB medium for 10 h at 37 ℃. Subsequently, 2.5 mL of seed culture was transferred into 50 mL of NM2 medium for the bioproduction. The fermentation process was conducted at 30 ℃ for 96 h. When required, IPTG and L-arabinose were added after 2 h. In the fed-batch culture, the initial glucose concentration was set to 10 g/L, and a concentration of 5 g/L glucose was fed every 12 h after the first 24 h of culture.

2.6. iso-Butylamine Production in a 7 L Bioreactor

A total of 100 mL of seed culture was transferred into a 7 L bioreactor (Parallel-Bioreactor, Shanghai, China) containing 2 L of NM2 medium. The initial glucose concentration was 15 g/L. The temperature was maintained at 37 ℃ for the first 8 h of fermentation, and then it was maintained at 30 ℃. After 12 h of culture, glucose was added at a constant feed rate of 3.3 g/L/h. The pH was maintained at approximately 6.8 using 25% (*v*/*v*) NH_4OH. The agitation speed was set between 250 rpm and 800 rpm throughout the process. Samples were taken during the process to determine OD_{600}, residual sugar concentration, and *iso*-butylamine production.

2.7. Analytical Methods

Cell growth was measured using an ultraviolet spectrophotometer (Yoke, Shanghai, China). The supernatant of the broth was collected by centrifugation at 12,000 rpm for 5 min to measure glucose and *iso*-butylamine. The glucose was quantified by the 3,5-dinitrosalicylic acid (DNS) assay [27]. Specifically, 100 μL of the sample was mixed with 200 μL

of DNS reagent and heated. Then, 900 μL of ddH_2O was added, and an OD_{540} was measured by a Multi-detection Microplate Reader (BioTek, Winooski, VT, USA).

The concentration of *iso*-butylamine was quantified using high-performance liquid chromatography (HPLC, Shimadzu, Kyoto, Japan, LC-20A). Before the measurement, precolumn derivatization of *iso*-butylamine was performed using *o*-phthaldialdehyde (OPA) [28]. For the derivatization, 100 μL of the sample was mixed with 500 μL of 0.40 M borate buffer and 100 μL of OPA derivatization reagent for reacting 2 min. Then, the mixture was injected into HPLC equipped with an Agilent zorbax SB C18 column (4.6 × 150 mm, 5 μm). The mobile phase consisted of solvent A (1.4 g/L of Na_2HPO_4, 3.8 g/L of $Na_2B_4O_7{\cdot}10H_2O$; pH 7.2) and solvent B (45% acetonitrile, 45% methanol, and 10% H_2O). The elution gradient was as follows: 0–0.5 min, 90% solvent A and 10% solvent B; 0.5–16.5 min, a linear gradient of B from 0 to 57%; 16.5–24.5 min, a linear gradient of B from 57 to 100%; 24.5–27.5 min, 100% solvent B; 27.5–29 min, a linear gradient of solvent B from 100 to 10%; 29–31 min, 10% solvent B. Flow rate and column temperature was 1 mL/min and 35 ℃, respectively. The detection wavelength of *iso*-butylamine was 338 nm.

2.8. Statistical Analysis

All data are presented as the mean ± standard deviation, with each experiment being conducted at least twice. Statistical comparisons were performed using the independent samples *t*-test to assess significant differences between the control and experimental groups.

3. Results

3.1. Combinatorial Optimization of Synthetic QS Circuits

To achieve sufficient fermentation production, it is crucial to switch metabolic modes between cell growth and bioproduct synthesis. In general, the *lux*-type QS system comprises three key components: acyl-homoserine lactone synthase LuxI, regulatory protein LuxR, and promoter P_{lux} [29]. In specific, the AHLs diffuse from the intracellular to extracellular until a specific concentration. Upon reaching this threshold, AHLs bind with the LuxR for forming the LuxR-AHL complex, thereby activating promoter P_{lux} (Figure 1A) [30]. Despite natural QS systems contributing to regulating physiological activities [31], their applications are often constrained by a narrow dynamic range and low response threshold [32]. To enhance their practical application, QS circuits require rational modifications for expanding the response range and tunable threshold.

To construct an artificial QS system with expanded dynamic range, essential regulatory elements were selected. Considering that promoter P_{lux} from *V. fischeri* is bidirectional, it is classified into P_{luxI} and P_{luxR}. To evaluate the transcriptional activities, two reporter plasmids, pRI and pRR, were constructed to serve as the response modules, with red fluorescent protein (mCherry) as a reporter. Meanwhile, genes *luxI/luxR* from *V. fischeri* ES114 were overexpressed under the medium-strength constitutive promoter P_{T5}, generating plasmid pSM1 (the sensory module). These plasmids were assembled to form different QS circuits. For one thing, strains QRR and QRI harboring the response module exhibited a low fluorescence, and in contrast, strains QMR1 and QMI1 harboring both sensory and response modules showed a higher fluorescence. These results indicated that the targeted gene was activated by complete QS circuits (Figure 1B). In particular, strain QMI1 harboring promoter P_{luxI} exhibited a 3.56-fold higher fluorescence than strain QMR1, suggesting promoter P_{luxI} has a higher transcriptional activity. Next, genes *luxI/luxR* with different amino acid sequences from another *V. fischeri* strain, JM11, were tested. As a result, dynamic range of the resultant strain QMI2 exhibited an improvement of 2.48-fold compared to strain QMI1 (Figure 1C,D). Additionally, strain QMI2 was characterized at various temperatures (30 ℃ and 37 ℃), and a higher dynamic range was observed at 30 ℃. Therefore, the following experiments were conducted at 30 °C (Figure S1). Overall, these results demonstrate that the integration of promoter P_{luxI} and genes *luxI/luxR* from *V. fischeri* JM11 enhanced dynamic range of the synthetic QS circuit.

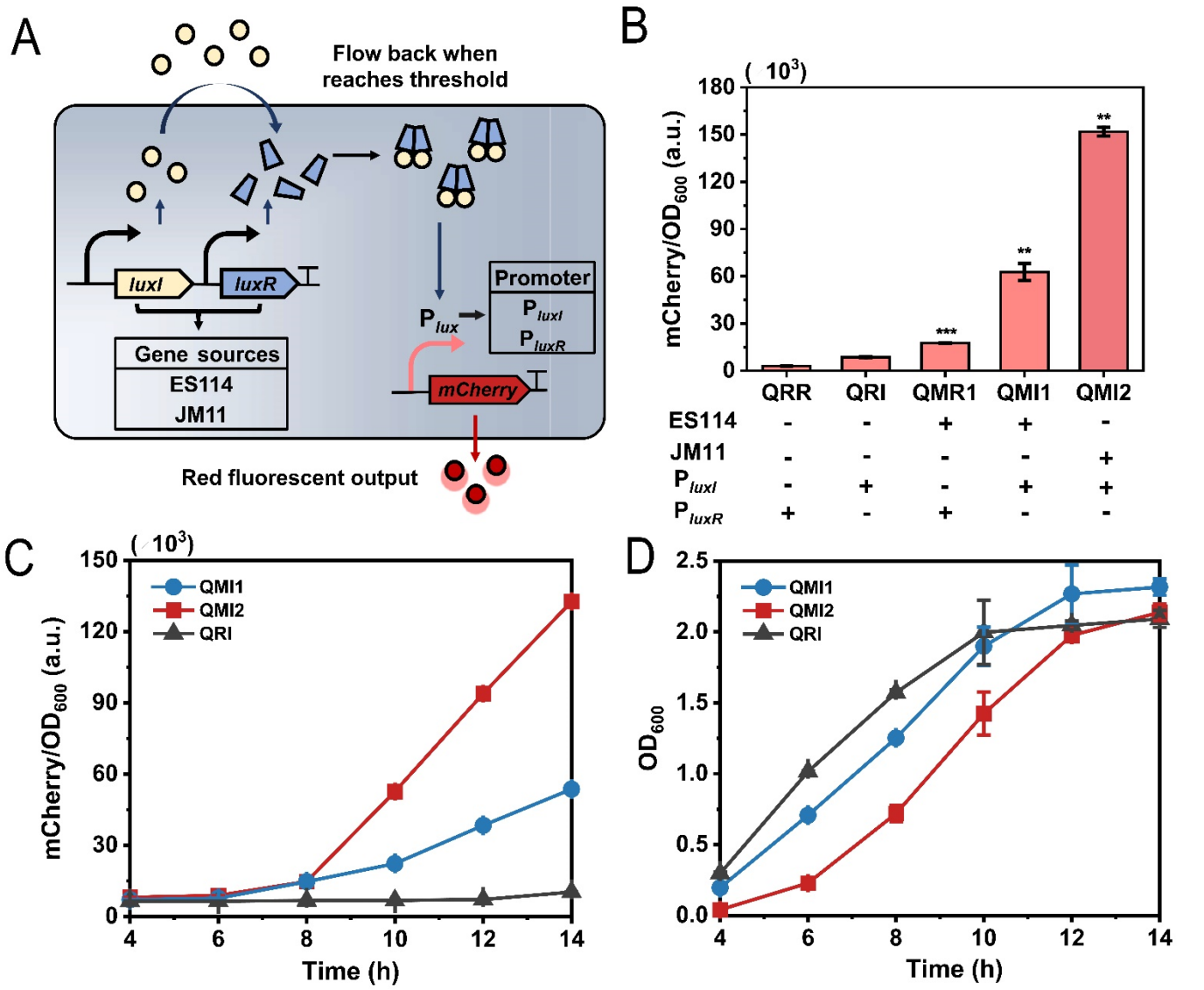

Figure 1. Element selection in constructing artificial QS systems. (**A**) Schematic diagram of QS circuit. Signaling molecules diffuse extracellularly at low cell density and reflux into the cell at high cell density, bind to LuxR to form complexes, and activate *mcherry* controlled by promoter P_{lux}. (**B**) Evaluation of artificial QS systems. The dynamic ranges of combinations of different *lux*-type promoter and *luxI/luxR* were grouped for altering the regulation characterization. (**C**) Fluorescence profiles in different engineered strains. Additionally, strain QRI containing only the response module served as the control. (**D**) Growth profiles in different engineered strains. The control strain QRI was also measured. Significant at different levels: ** $p < 0.01$, *** $p < 0.001$.

To alter the triggering threshold of artificial QS systems, the expression of genes *luxI/luxR* was systematically optimized. Previous studies have shown that adjusting AHLs accumulation can influence triggering OD_{600}. Considering that available LuxR is required for the functionality, the intracellular LuxR level may also impact the performance. Therefore, modular engineering was used to enhance regulation performance by employing promoters of different strengths, yielding strains QMI3–QMI10 (Figure 2A). Indeed, this approach yielded QS systems with diverse properties. On one hand, the triggering OD_{600} (1.62~1.80) of these strains exhibited an increase compared to strain QMI2, accompanied by diverse dynamic ranges (Figure 2B,C). For instance, the circuit was activated at a higher OD_{600} (~2.09) through a synergetic combination of strong *luxR* and moderate *luxI* expression (strain QMI10), nearing the stationary phase. In particular, the decreased *luxI* expression effectively increased triggering OD_{600}, whereas the reason remained unclear for higher *luxI* expression, which still switched at a high OD_{600}. A previous study confirmed that the triggering OD_{600} does not always correlate linearly with AHLs output [33]. Kim's study showed that although low *luxI* expression delayed the activation, its higher expression did not lead to earlier triggering [21]. Moreover, we speculated that the approach in altering response threshold was limited by manipulating *luxI/luxR*. In addition, the mechanism of AHL-LuxR activation process has been elucidated, while the research on the kinetics of complex formation remains scarce. Taken together, the performance of QS systems was successfully modified, alongside with dynamic ranges and

triggering OD_{600}.

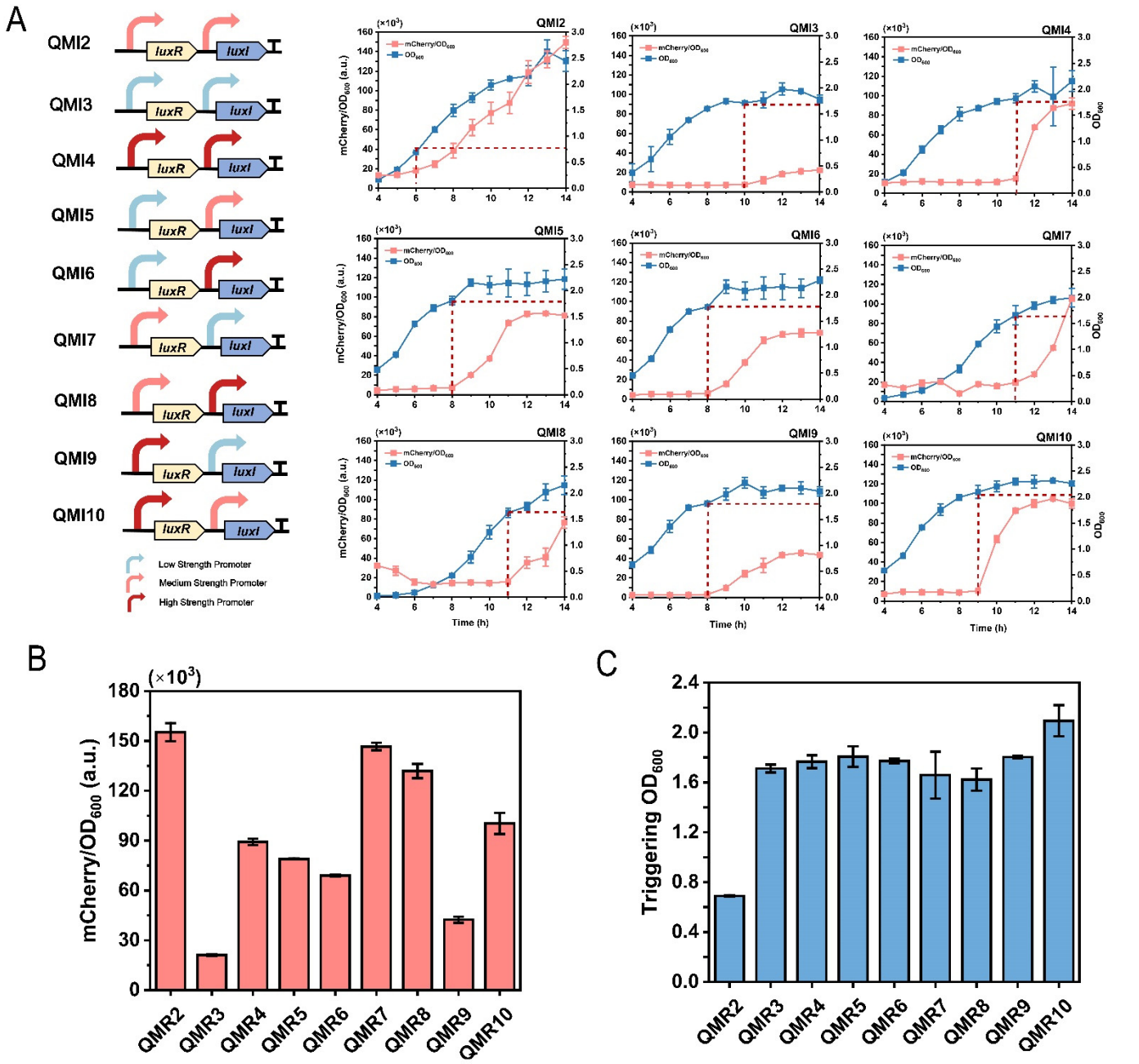

Figure 2. Promoter engineering for the optimization of QS circuit. (**A**) Schematics diagram for engineering sensor modules with different promoters. The red dotted lines in the profiles indicate the time and corresponding OD_{600} of QS activation. (**B**,**C**) Dynamic ranges (**B**) and triggering OD_{600} (**C**) of several engineered strains.

3.2. Screening the LuxR Variant Insensitive to AHLs

To provide a broader selection of QS circuits susceptible to metabolic regulation, more diverse QS systems with varied performances are required. In the aforementioned study, only one QS circuit triggered activation at the OD_{600} of 2.09, further efforts ought to be made to develop variable QS circuits capable of triggering at a high OD_{600}. Given that all the *luxI/luxR* cassette combinations have been characterized, a new approach was required to obtain QS circuits with different performances by refactoring transcription factor [34]. In this study, we aimed to engineer QS circuits with unique properties and high triggering OD_{600} by developing LuxR mutants with lower sensitivity to AHLs.

To obtain LuxR mutants with reduced AHLs sensitivity, random mutation and "ON/OFF" screening were applied. LuxR, an allosteric protein, consists of an *N*-terminal region and a *C*-terminal domain, which are responsible for binding autoinducer and the specific DNA sequence to activate promoter P_{lux}, respectively [35–37]. In this study, we targeted the amino acid sequences between residues 23 to 147 for modification through the error-prone PCR. First, plasmid

pLuxR was constructed by deleting *luxI* of plasmid pSM10 to eliminate endogenous interference. This ensured that the mutations affected the sensitivity to AHLs without reducing DNA affinity. Subsequently, different concentrations of 3OC6HSL were exogenously added, and it was found that the wild-type LuxR required 19.97 nM 3OC6HSL for half-maximal luminescence, with peak expression occurring at 100 nM (Table 1, Figure 3C). Therefore, 100 nM 3OC6HSL was added in the "OFF" screening to identify mutants with low affinity for 3OC6HSL. In the first round of screening, a library of 728 mutants was tested, and 76 non-luminescent candidates were identified (Figure 3B). To minimize experimental variability and exclude inactive mutants, the "ON" screening was conducted by exogenously adding 100 nM and 10,000 nM of 3OC6HSL. At the high concentration of 10,000 nM, those mutants failing to express fluorescence were classified as the non-function [24]. Several mutants, however, exhibited a significantly higher fluorescence at 10,000 nM than at 100 nM (Figure 3C). Sequencing analysis revealed that the generated five mutants possessed several amino acid mutations (Table 1). Subsequently, the AHL-dependent activation of these mutants was evaluated across a range of 3OC6HSL concentrations. As expected, fluorescence curves showed that all variants could be activated at a higher concentration of 3OC6HSL. Among them, variant M3 (V36E/H89L/P97L) exhibited the lowest sensitivity, with a $[3OC6HSL]_{50}$ of 5314.83 nM. Additionally, two other mutants, M2 (C38Y/Y47C/I76M) and M3 (E112G), also exhibited similar $[3OC6HSL]_{50}$. In contrast, variant M5 (N88D) showed sensitivity only slightly lower compared to the wild type. Overall, several mutants with decreased sensitivity ranging from 1.72 to 266.14 times have been identified.

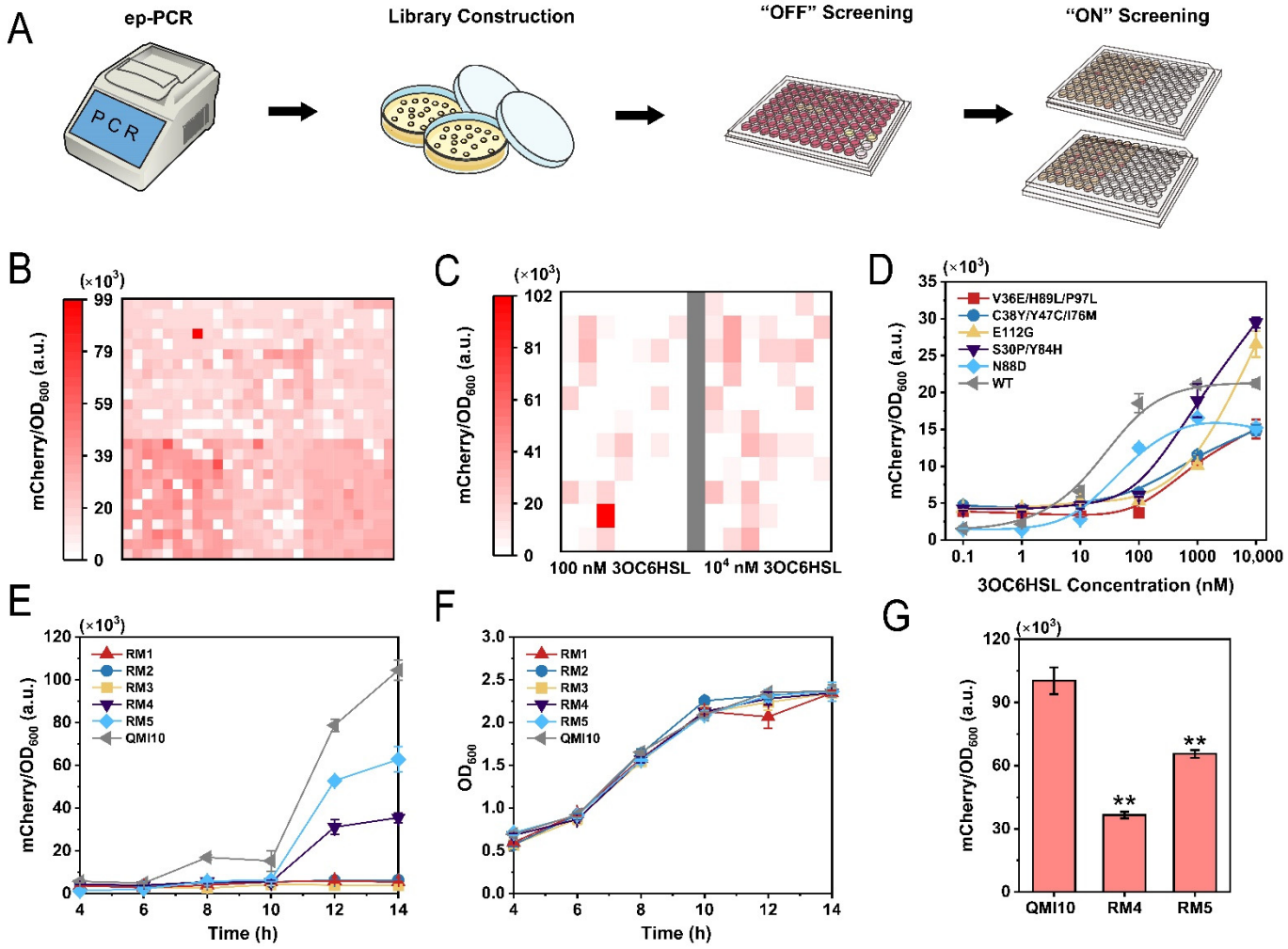

Figure 3. The screening of LuxR mutants with reduced sensitivity to AHLs. (**A**) Schematic diagram for constructing and screening LuxR mutant library. (**B**) The "OFF" screening for LuxR mutants at 100 nM of 3OC6HSL. (**C**) The "ON" screening for LuxR mutants. The fluorescence outputs of candidates after the addition of 100 nM and 10,000 nM 3OC6HSL are presented on the left and right sides of the grey column, respectively. Strains at the corresponding positions are identical. (**D**) Fluorescence profiles of LuxR mutants at different concentrations of 3OC6HSL. (**E**,**F**) Time-course profiles of LuxR mutants. (**E**) Normalized mCherry fluorescence, (**F**) Cell growth. (**G**) Dynamic ranges of LuxR mutants. Significant at different levels: ** $p < 0.01$.

Table 1. The nucleotides substitutions, amino acids substitutions and dissociation constants of LuxR variants.

LuxR Variant	Nucleotides Substitution	Amino Acids Substitution	$[3OC6HSL]_{50}$ (nM) [a]
WT	NA [b]	NA	19.97
M1	T107A, T183C, A266T, T291A	V36E, H89L, P97L	5314.83
M2	G113A, A140G, A170G, A228G	C38Y, Y47C, I76M	4814.62
M3	A335G	E112G	4326.19
M4	T88C, T250C	S30P, Y84H	547.73
M5	A262G	N88D	34.42

[a] $[3OC6HSL]_{50}$ represents the concentration required for reaching half-maximal luminescence level, namely the dissociation constants of every variant. The values are obtained by fitting to Hill equations. [b] "NA" stands for "Not Available".

3.3. LuxR Variants Characterization in Complete QS Circuits

Given that LuxR variants displayed different fluorescence levels at a high concentration of 3OC6HSL (10,000 nM), we further evaluated the performance of these mutants within complete QS circuits. In specific, these variants were introduced into strain QMR10 for yielding strains RM1–RM5. Fluorescence profiles indicated that only two variants (RM4 and RM5) exhibited the fluorescence without exogenous 3OC6HSL (Figure 3E–G). However, they exhibited lower dynamic ranges compared to strain QMR10. Given that LuxR is unstable when not bound to AHLs, we speculated that the reduced sensitivity prevented the mutants from timely binding to AHLs, leading to less soluble LuxR to activate promoter P_{luxI}.

For the other three variants that failed to the activation by autoinduction, to examine if they had become inactive during the mutation introduction, exogenous 10,000 nM of 3OC6HSL was added, and it resulted in markedly higher fluorescence compared to the control (Figure S2A). A possible explanation for the decreased performance might be attributed to the following aspects: (i) strain QMI10 harboring the wild-type LuxR was able to activate QS circuit, while strains RM1–RM3 failed under the similar OD_{600} (Figure S2B); (ii) these mutants possessed a 200-fold lower AHLs sensitivity at the *in vitro* assays. Taken together, we speculated that inadequate biomass could not activate the complete QS circuit in shaking flasks. In further research, the characterization of LuxR mutants with extremely low sensitivity can be conducted in a larger-scale system.

3.4. Digging Out Metabolic Bottleneck in De Novo Synthesis of iso-Butylamine

iso-Butylamine, a short-chain primary amine, is highly valued in organic synthesis and extensively used as a pesticide raw material [38]. Nowadays, its industrial production requires costly reagents and harsh reaction conditions, which often lead to low yield and poor stereoselectivity. As an alternative, the biosynthesis offers a more sustainable and environment-friendly method, whereas the study remains limited. Until recently, microbial platform for *iso*-butylamine bioproduction was established by expanding pyruvate catabolism and introducing valine decarboxylase (*vlmD*) from *Streptomyces viridifaciens* for the first time, while it merely yielded low bioproduct titer due to the unknown factors [39].

In a previous study, our group constructed an *iso*-butylamine biosynthetic platform and validated the feasibility of *de novo* synthesis with glucose as the sole carbon source. For the purpose of enhancing the efficiency of chassis IB01, several strategies were performed (Figure 4). Firstly, we speculated that a low titer of bioproduct might be attributed to insufficient L-valine supply. Several studies have indicated that overexpression of leucine-responsible regulator protein (Lrp) can improve L-valine titer by activating the *ygaZH* efflux transporter and *ilvIH*, an isozyme of *ilvBN* [40]. Therefore, plasmid pLRP was constructed by overexpressing *lrp*, yielding strain IB02, while the generated titer was only 1.90 g/L in shaking flasks, comparable to strain IB01 (1.87 g/L). Subsequently, the competitive pathways involved in pantothenate, L-leucine, and L-isoleucine synthesis were attempted for down-regulating by RNA interference (RNAi), which enabled improvement of intracellular 2-ketoisovalerate pools [41]. However, the titer remained low at 1.86 g/L in strain IB03. Taken together, these results indicate that overexpression of *lrp* and simple competitive pathway suppression may not be the limiting factors for a high-level synthesis.

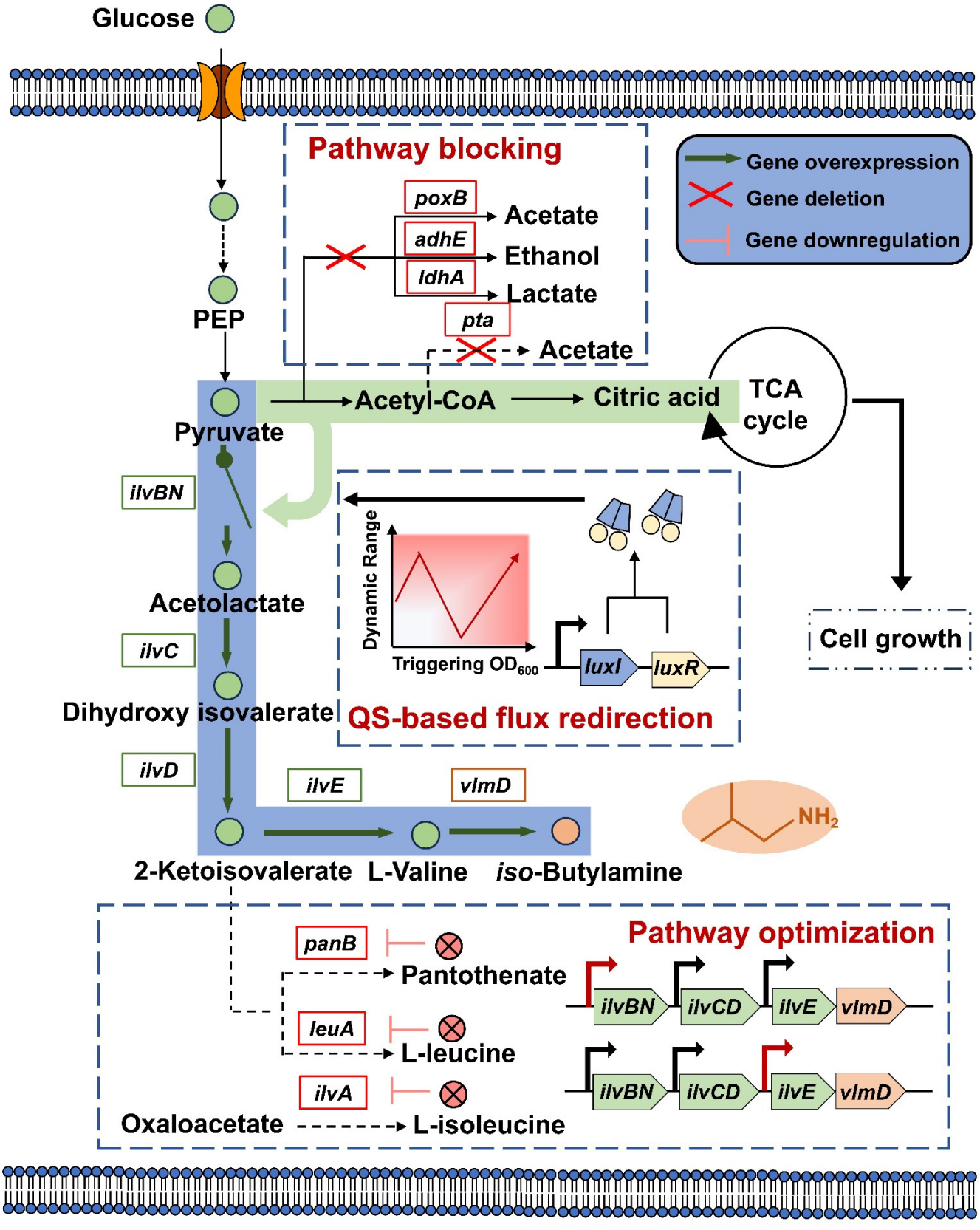

Figure 4. Metabolic engineering of *iso*-butylamine synthesis in *E. coli.* The pathway with the blue background is the *iso*-butylamine pathway, while the green background represents the central pathway. Genes in green, orange, and red boxes indicated endogenous genes, heterologous genes, and the knockout or down-regulation. Abbreviation: PEP, phosphoenolpyruvate. Genes: *poxB*, pyruvate oxidase; *adhE*, alcohol dehydrogenases; *ldhA*, lactate dehydrogenase; *ilvB*, acetohydroxy acid synthase I large subunit; *ilvN*, acetohydroxy acid synthase I small subunit; *ilvC*, ketol-acid reductoisomerase; *ilvD*, dihydroxy-acid dehydratase; *ilvE*, branched-chain-amino-acid aminotransferase; *pta*, phosphate acetyltransferase; *ilvA*, L-threonine dehydratase; *panB*, pantothenate synthase; *leuA*, 2-isopropylmalate synthase.

Next, we focused on reinforcing metabolic fluxes by enhancing *ilvBN* expression. Specifically, the medium-strength of promoter P_{trc} was substituted by a stronger promoter P_{J23119}, and the resultant strain was redesignated as IB04. As shown in Figure 5B, strain IB04 achieved a titer of 3.36 g/L, representing a 79.68% improvement over strain IB01. Additionally, the conversion efficiency of L-valine to *iso*-butylamine was improved by enhancing *vlmD* expression in strain IB05, resulting in a titer of 2.21 g/L. Therefore, the elevated carbon flow driven by *ilvBN* is beneficial for achieving a high-level of bioproduct, underscoring the significance of sufficient pyruvate supply.

To verify whether the pyruvate supply is the bottleneck in *iso*-butylamine synthesis, pyruvate was exogenously supplied [42]. Considering that strain IB01 possessed the non-optimal pathway, its evaluation may be more significantly impacted. With the increased concentration of extracellular pyruvate, the titer of *iso*-butylamine increased, and the cell growth was not affected (Figures 5C and S3). It indicated that the increased production was attributed to adequate pyruvate supply. Overall, these findings confirm that unavailable intracellular pyruvate is one of bottlenecks in *iso*-butylamine synthesis.

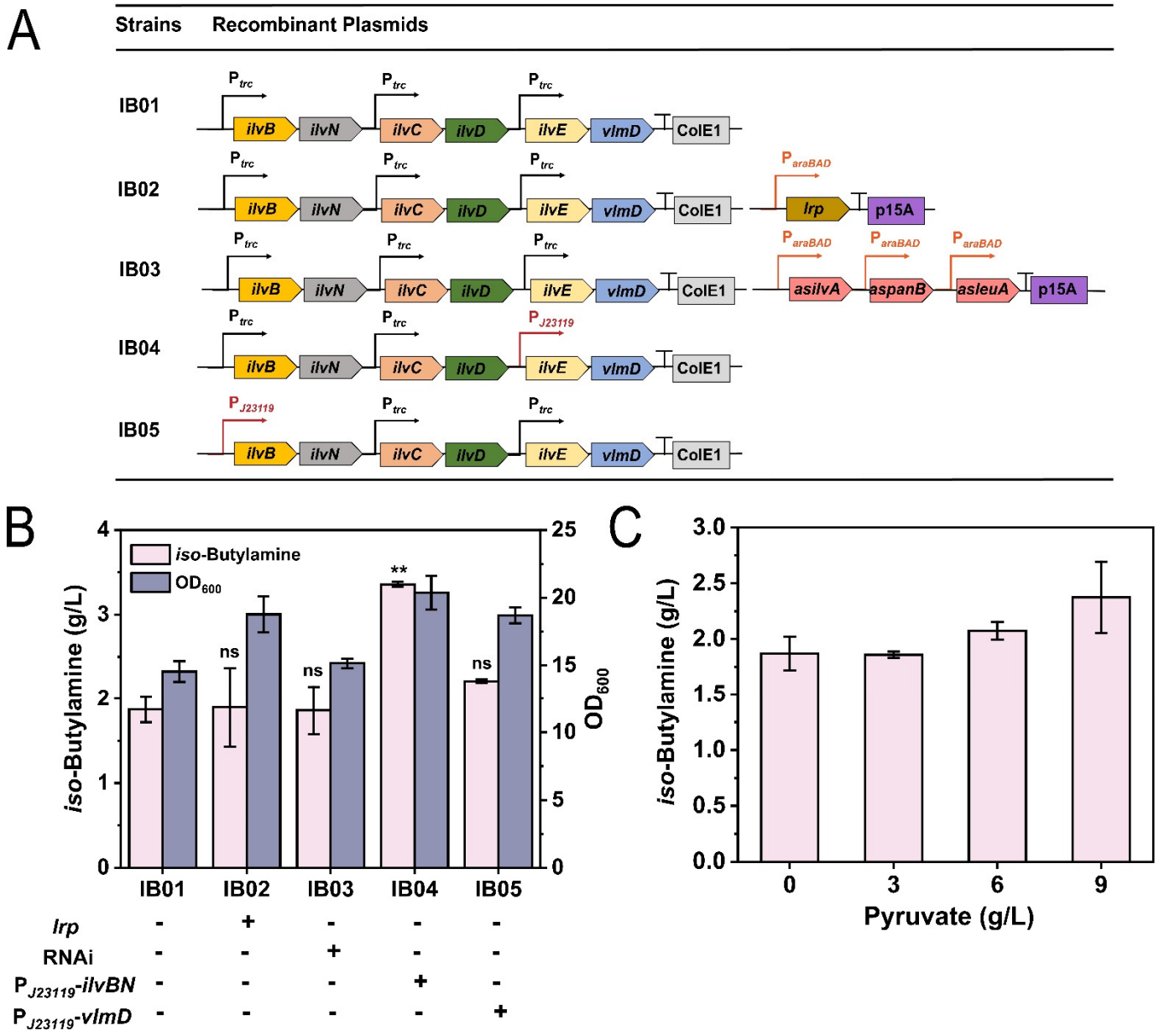

Figure 5. Microbial engineering for *iso*-butylamine synthesis. (**A**) Schematic diagram of engineered strains with static modification. (**B**) *iso*-Butylamine titers and OD_{600} of engineered strains. (**C**) Effect of exogenous pyruvate addition on *iso*-butylamine synthesis in strain IB01. Significant at different levels: ** $p < 0.01$, ns $p > 0.05$.

3.5. Efficient Synthesis of iso-Butylamine by Modular QS Circuits

To redirect pyruvate towards *iso*-butylamine synthesis, synthetic QS circuits were introduced to balance cellular resources between cell growth and *iso*-butylamine production. The whole process was divided into two stages (Figure 6A). In the first stage, pyruvate was channeled into acetyl-CoA to support energy production and cell growth requirements (growth stage). After sufficient biomass accumulation, QS circuits activated the *iso*-butylamine pathway and redirected pyruvate towards the bioproduction (synthesis stage). This staged approach allows for optimized resource allocation, with QS circuits coordinating the transition from growth to production phases to maximize *iso*-butylamine titer.

To achieve dynamic control of pyruvate catabolism, the previously optimized QS systems were introduced into strain IB00 by replacing *mcherry* with *ilvBNCDE* and *vlmD* on plasmid pRI. A series of quorum sensing systems with different regulatory characteristics were previously constructed (Table 2). In total, eight QS systems with distinct performances were selected to identify the optimal regulatory approach. The dynamic ranges and thresholds of these systems were categorized into low, medium, and high levels. The performance of these systems was evaluated in NM2 medium to minimize the impact of medium components, and there was no significant difference observed (Figure S4). Initially, the effectiveness of the QS systems derived from strains QMI1 and QMI2-characterized by low thresholds and medium or high dynamic ranges, was evaluated. As shown in Figure 6B, strain IB13, which utilized a QS system with a high dynamic range, yielded 8.19 g/L *iso*-butylamine, representing a 143.75% increase compared to the static control. However, it exhibited extremely low biomass accumulation. In contrast, strain IB12, equipped with a medium dynamic range, demonstrated improved cell growth. This suggests that the enhanced pathway during the early growth stage diverted overabundant pyruvate towards *iso*-butylamine synthesis, thereby impeding cell growth. However, strain IB12 only produced 4.13 g/L product, approximately half the titer of strain IB13, indicating that a higher dynamic range was more beneficial for optimal titer improvement. These results highlighted the importance of fine-tuning metabolic flux between growth and product synthesis. To address the trade-off between metabolic burden and product yield, activation time of the QS systems was strategically delayed. Thereby, QS systems with high triggering OD_{600} were applied, derived from strains RM4, RM5 and QMI10, generating strains IB31, IB32 and IB33. Compared to the initially tested systems, these strains displayed improved cell growth due to the delayed activation of metabolic pathways. Notably, strain IB33 harboring a combined high dynamic range with delayed activation, achieved a titer of 9.47 g/L, representing a 15.63% improvement over strain IB13. Furthermore, QS systems characterized with medium thresholds, sourced from strains QMI3, QMI9 and QMI4, were also evaluated. Surprisingly, strain IB21, characterized by a low dynamic range, achieved the highest yield of 10.79 g/L, surpassing strain IB33 by 13.94%. A possible explanation for improved titer might be that the delayed and low-level expression of pathway genes alleviated the toxicity, thereby fostering a more conducive metabolic environment for *iso*-butylamine production. These findings underscore that QS regulation is a dynamic and finely tuned process, and optimal production could only be achieved by employing the most suitable approach.

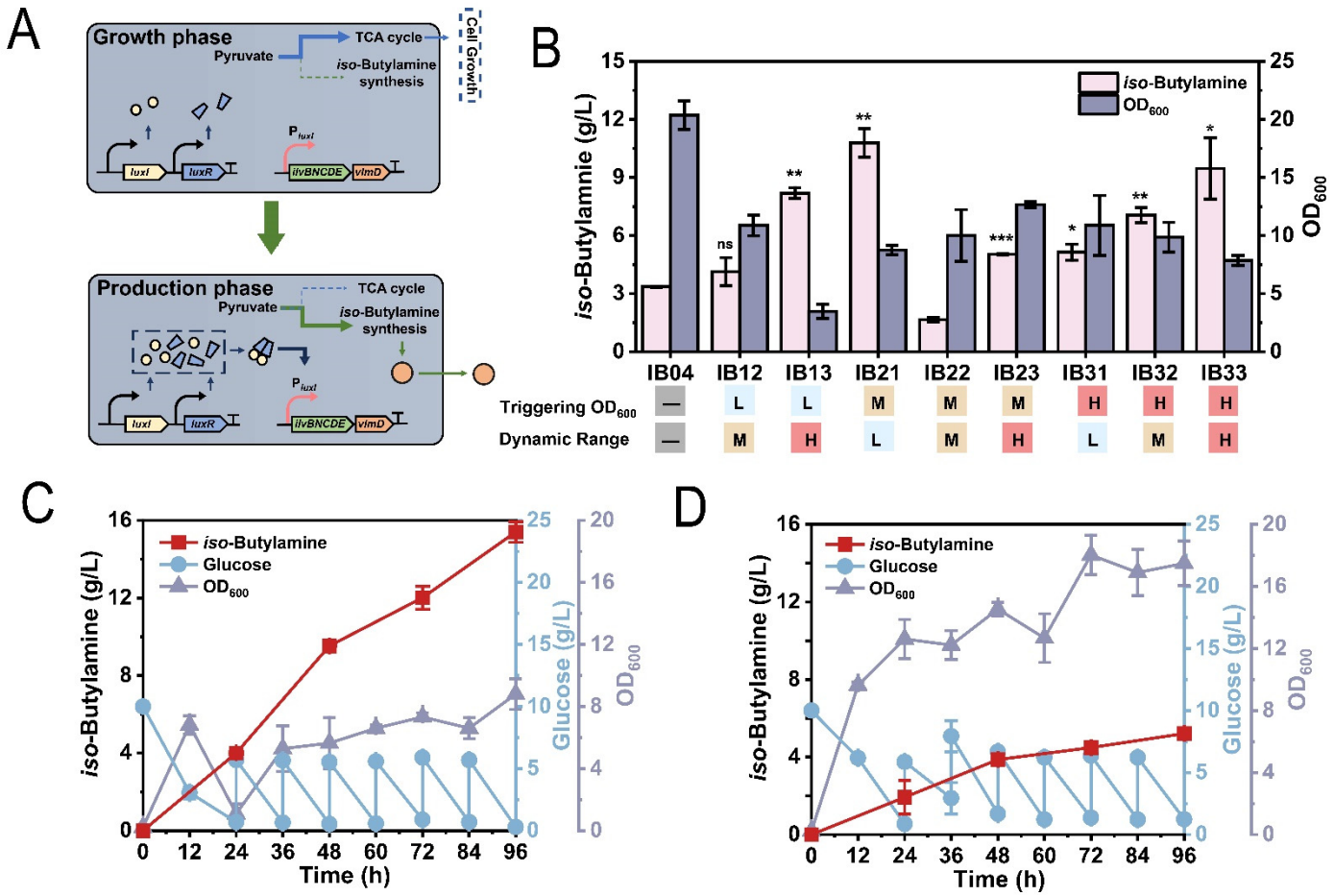

Figure 6. Dynamic control of *iso*-butylamine synthesis. (**A**) Schematic diagram of QS-based *iso*-butylamine producing strains. Pyruvate flux was diverted into TCA cycle to support cell growth during growth phase. According to the introduced QS system, when cell density reaches a specific threshold, pyruvate flux was redirected into *iso*-butylamine synthesis with varying intensities. (**B**) Effects of QS systems on *iso*-butylamine production. "L", "M", and "H" individually represent the level of triggering OD_{600} and dynamic range, and "-" stands for static control. (**C**,**D**) The fermentation profiles in strains IB21 (**C**) and IB04 (**D**) during the fed-batch fermentation. Significant at different levels: * $p < 0.05$, ** $p < 0.01$, *** $p < 0.001$, ns $p > 0.05$.

Table 2. The properties of diverse QS systems.

QS System	Triggering OD_{600}	Fold Change [a]	Dynamic Range (a.u.)	Fold Change [b]
QMI1	0.70	0	62,693.08	0
QMI2	0.69	−0.014%	155,265.80	+147.66%
QMI3	1.71	+144.29%	21,050.01	−66.42%
QMI4	1.76	+151.43%	89,257.24	+42.37%
QMI5	1.81	+158.57%	78,945.42	+25.92%
QMI6	1.77	+152.86%	69,003.55	+10.07%
QMI7	1.79	+155.71%	146,614.00	+133.86%
QMI8	1.69	+141.43%	131,899.50	+110.39%
QMI9	1.81	+158.57%	42,411.51	−32.35%
QMI10	2.09	+198.57%	100,312.10	+60.01%
RM4	2.13	+204.29%	36,526.55	−41.74%
RM5	2.09	+198.57%	65,553.60	+4.56%

[a, b] They represent the degree of change in the triggering OD600 and dynamic ranges of the QS systems compared to strain QMI1, respectively.

To further improve the efficiency of *iso*-butylamine synthesis, other strategies were employed to optimize pyruvate availability as well. For one thing, pyruvate is primarily channeled into the TCA cycle to provide reducing power and energy for cell growth due to robust central metabolism [43]. For another thing, native glucose transport mediated by the phosphotransferase system (PTS) inevitably consumes PEP, limiting available pyruvate. Based on these insights, strain IB21A was engineered to down-regulate TCA cycle by targeting citrate synthase (encoded by *gltA*) using RNAi,

and the PTS was replaced by glucose facilitator and glucose kinase (encoded by *glf* and *glk*) from *Zymomonas mobilis* to generate strain IB21B [41]. Unfortunately, a dramatic reduction in titer was observed compared to strain IB21, yielding 8.02 g/L and 1.29 g/L for strains IB21A and IB21B, respectively (Figure S5). Taken together, impaired primary metabolism seriously affects physiological metabolism and the decreased titer.

To prolong the growth phase and boost product titer, the fermentation mode was optimized by feeding a low glucose concentration at multiple intervals. As a control, static control induced by IPTG was performed in strain IB04. As a result, a total of 40 g/L glucose was consumed (Figure 6C,D). However, strain IB12 achieved a final titer of 15.40 g/L in spite of accumulating less biomass compared with strain IB04, displaying a 2.96-fold increase over the static control. Importantly, its yield reached 0.39 g/g, significantly surpassing strain IB04. As a control, the constitutive promoter P_{trc} was used to control *iso*-butylamine pathway, while it only accumulated 2.73 g/L of *iso*-butylamine and exhibited low biomass accumulation and glucose consumption in strain IB06, equivalent to 17.73% of strain IB21 (Table 3). Moreover, continuous expression negatively impacted microbial physiological metabolism, alongside with decreased growth rate and product synthesis. In contrast, the superiority of QS system was highlighted. Taken together, the QS system not only enhances yield and productivity but also maintains metabolic balance, underscoring its role in optimizing bioprocess efficiency.

Table 3. *iso*-Butylamine synthesis in different control modes.

Strain	Regulation Strategy	Titer (g/L)	Yield (g/g)	Productivity (g/L/h)	OD_{600}	Consumed Glucose (g/L)
IB21	QS regulation	15.40	0.39	0.16	8.80	39.71
IB04	IPTG induction	5.21	0.13	0.05	17.46	38.76
IB06	Constitutively	2.73	0.21	0.03	5.63	12.81

3.6. Production of iso-Butylamine in a 7 L Bioreactor

The optimal strain IB21 was evaluated for the *iso*-butylamine production capacity in a 7 L bioreactor. As illustrated in Figure 7, the initial glucose was nearly exhausted at 12 h, after which the residual glucose concentration was maintained at a low level by continuous feeding. After the fermentation period of 96 h, a total of 276.86 g/L of glucose was consumed, and the highest titer of *iso*-butylamine (44.23 g/L) was accumulated in strain IB21, displaying a 2.87-fold improvement compared to that in shaking flasks. In addition, its yield and productivity reached 0.16 g/g and 0.46 g/L/h, respectively. Overall, it demonstrated that the efficient QS system significantly boosted *iso*-butylamine production, indicating its potential for industrial bioproduction applications.

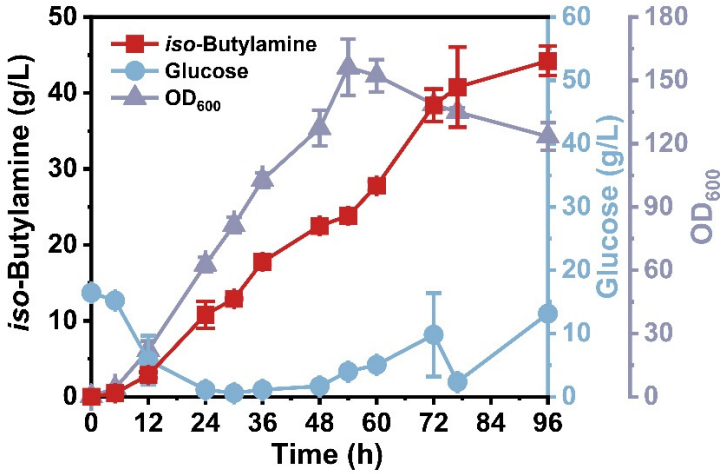

Figure 7. Efficient production of *iso*-butylamine in a 7 L bioreactor by strain IB21. The glucose concentration was maintained at a low level after the initial addition was exhausted, through continuous feeding with a rate of 3.33 g/L/h.

4. Discussion and Conclusions

To optimize bioproduct synthesis, microbial cell factories necessitate precise metabolic regulation. However, the limited QS toolkits restrict widespread applicability. In this study, a versatile suite of QS systems was designed by screening key regulatory components, conducting combinatorial optimization, and refactoring the regulatory factor. On one hand, a synthetic QS circuit with high dynamic range was engineered by combining promoter P_{luxI} and genes

luxI/luxR from *V. fischeri* JM11. In particular, QS circuits with elevated response thresholds and tailored dynamic ranges were constructed by modulating the *luxI/luxR* expression. On the other hand, novel variants that reduced the affinity of LuxR for AHLs were identified for high-threshold circuit construction. Finally, significant product titer, yield, and productivity were generated after applying in controlling *iso*-butylamine synthesis compared to the static control. These highlight the potential of QS-mediated dynamic regulation in enhancing the efficiency and scalability of bioproduction process.

The established QS circuit with diverse properties expands genetic toolkits. Currently, the efforts in modifying QS circuits predominantly focus on enhancing dynamic range, adjusting the threshold, and minimizing leaky expression by combinatorial optimization and genetic elements refactoring [20,44,45]. Previous studies have successfully elevated dynamic range by optimizing expression components, such as promoters, RBS, and copy number [21,46]. However, limited efforts in threshold have been obtained [32]. More recently, the CRP-binding sites of promoter P_{luxI} offered an innovative solution for improving the performance, in which QS circuits with diverse thresholds were generated, increasing the triggering threshold by 1.61-fold to reach 1.437 [23]. Another study achieved a 1.5 to 3.6-fold increase in triggering OD_{600} through random mutagenesis of promoter P_{luxI} [47]. Although variant C77T elevated the triggering OD_{600}, it was still within the early growth phase. In this study, combinatorial optimization was conducted, and the threshold was improved by 2.45- to 3.03-fold, achieving a maximum triggering OD_{600} of 2.09. The identified variants demonstrated a decreased AHLs sensitivity ranging from 1.72 to 266.14-fold. Specifically, a triple mutant V36E/H89L/P97L exhibited the lowest sensitivity with a dissociation constant of 5314.83 nM. Several high-threshold QS circuits were constructed based on these mutants, substantially expanding the pool of QS circuits. This work not only provides a tunable suite of QS circuits but also establishes a foundation for designing regulatory tools with tailored properties, offering greater flexibility for metabolic engineering applications.

A fully autonomous and pathway-independent regulatory tool for metabolic regulation has been established. Despite the fact that static control is effective in achieving high bioproduct titer, yield, and productivity, several challenges still persist. For example, redirecting metabolic flux to enhance synthesis may disrupt cellular homeostasis. Moreover, certain specific pathway intermediates or enzymes may require temporally controlled expression or utilization to improve the biosynthesis of the target product [6]. Dynamic regulation offers a promising method to address these conflicts. Recent advances have demonstrated the utility of biosensors responding to certain metabolites in regulating metabolic flux [48]. For instance, a pyruvate biosensor was applied to downregulate central metabolism and activating glucaric acid production in *Bacillus subtilis*, resulting in a 154% improvement in titer [49]. Also, there are lots of examples applying biosensors responsive to metabolites like malonyl-CoA, theophylline, and glycine [50–52]. However, these approaches are pathway-dependent, and available response elements are lacking. As an alternative, the biosensors responsive to temperature, pH, and oxygen have been developed, whereas these systems require human intervention to monitor and adjust the environmental conditions, and their efficiency may be unstable [53–55]. However, these systems require human intervention and exhibit unstable efficiency [56]. In contrast, this study leveraged QS circuit to design the regulatory tool for metabolic regulation. These designed QS circuits respond to different cell densities without human supervision, enabling fully autonomous regulation. Importantly, QS circuits operate independently of specific metabolic pathways, making them universally applicable for regulating diverse biosynthetic processes. These characteristics position QS circuit as a versatile and powerful tool for metabolic engineering, offering broad applicability across various bioproduction scenarios.

A QS-based platform was established to redirect pyruvate flux towards *iso*-butylamine synthesis dynamically. As one of the L-valine derivatives, pyruvate is a key precursor for *iso*-butylamine synthesis. Given its central metabolite role, insufficient supply usually limits product titer [57]. To enrich the pyruvate pool, strategies such as redirecting carbon flux, enhancing glycolytic flux, and blocking competitive pathways have been conducted [58]. However, conventional approaches involved TCA cycle disruption, auxotrophy and ATP/cofactor engineering lack flexibility, thus impairing metabolic balance and leading to suboptimal outcomes [59–61]. Recently, dynamic regulation has emerged as a promising alternative, enabling precise metabolic control in pyruvate-derived biosynthesis. Current *iso*-butylamine synthesis relies on static modifications, with limited metabolic pathway analysis and a relatively low titer of 10.67 g/L [39]. This study demonstrates that QS-based dynamical regulation can overcome these limitations, offering a more flexible and efficient approach to pyruvate flux management for enhanced *iso*-butylamine production. Through systematic pathway optimization, pyruvate supply was identified as one of the bottlenecks in *iso*-butylamine production. Subsequently, the application of QS increased the titer by 1.23- to 3.21-fold over the optimal static control, though redirecting the pyruvate into the target pathway in an appropriate manner. The superior performance of QS-based engineered strain was evident, as it outperformed both IPTG-induced and constitutively expressing strains. Notably, this strain achieved a remarkable titer of 44.23 g/L in a bioreactor, setting a new benchmark for *de novo iso*-butylamine

synthesis. Additionally, this process no longer requires exogenous inducers, thereby reducing production costs. Our work demonstrates that QS circuit-mediated dynamic regulation, compared to static control, can effectively and rationally allocate intracellular resources, thereby promoting microbial production. Moreover, this work also highlights the potential of QS circuits as a versatile tool for pyruvate-derivative production, offering a promising strategy for the production of other valuable bioproducts production.

In summary, this study significantly expands the toolbox of available QS circuits and demonstrates a promising approach for enhancing the value-added chemical biosynthesis. However, several challenges require further attention. Firstly, although QS circuits with different regulatory performances were obtained by modifying LuxR, novel or more functionally diverse QS components should be developed to meet various needs. Secondly, the characterization of QS circuits is currently limited to shaking flasks, yet some parameters of QS circuits, such as response threshold, cannot be significantly increased. Therefore, it is necessary to study QS circuits in a bioreactor for future research. Additionally, precise control of fermentation parameters should be thoroughly investigated to enhance the overall efficiency of *iso*-butylamine biosynthesis, and exploring the optimal fermentation conditions may further enhance the yields, offering avenues for future optimization.

Supplementary Materials

The following supporting information can be found at: https://www.sciepublish.com/article/pii/535, Table S1. The plasmids used in this study; Table S2. The strains used in this study; Table S3. The primers used in this study; Table S4. Amino acid sequences of heterologous genes; Figure S1. Dynamic range of strain QMI2 at different temperatures. Figure S2. The characterization of LuxR mutants failing to self-induce; Figure S3. Growth profiles of strain IB01 with exogenous pyruvate addition; Figure S4. The characterization of selected QS systems for regulation of *iso*-butylamine synthesis; Figure S5. Effects of increasing pyruvate supply by downregulating TCA cycle or reconstructing non-PTS glucose transportation system on the titer.

Author Contributions

Conceptualization, Y.L., M.L. and J.W.; Methodology, Y.L. and M.L.; Validation, M.L. and Y.L.; Formal Analysis, M.L. and Y.L.; Investigation, M.L. and Y.L.; Resources, Y.L., M.L., P.Y. and J.W.; Data Curation, M.L.; Writing—Original Draft Preparation, M.L.; Writing—Review & Editing, Y.L., M.L., H.F. and J.W.; Visualization, M.L.; Supervision, J.W.; Project Administration, J.W.; Funding Acquisition, J.W.

Ethics Statement

Not applicable.

Informed Consent Statement

Not applicable.

Data Availability Statement

Data will be made available on request.

Funding

This research was supported by the National Natural Science Foundation of China (22178133) and Guangdong Provincial Key Research and Development Program (2024B1111160006).

Declaration of Competing Interest

The authors declare that they have no known competing financial interests or personal relationships that could have appeared to influence the work reported in this paper.

References

1. Liu H, Qi Y, Zhou P, Ye C, Gao C, Chen X, et al. Microbial physiological engineering increases the efficiency of microbial cell factories. *Crit. Rev. Biotechnol.* **2021**, *41*, 339–354.
2. Zhao C, Zhao Q, Li Y, Zhang Y. Engineering redox homeostasis to develop efficient alcohol-producing microbial cell factories.

Microb. Cell Fact. **2017**, *16*, 115.
3. Fatma Z, Hartman H, Poolman MG, Fell DA, Srivastava S, Shakeel T, et al. Model-assisted metabolic engineering of *Escherichia coli* for long chain alkane and alcohol production. *Metab. Eng.* **2018**, *46*, 1–12.
4. Wu J, Zhou P, Zhang X, Dong M. Efficient *de novo* synthesis of resveratrol by metabolically engineered *Escherichia coli*. *J. Ind. Microbiol. Biotechnol*. **2017**, *44*, 1083–1095.
5. Keasling JD. Manufacturing molecules through metabolic engineering. *Science* **2010**, *330*, 1355–1358.
6. Ni C, Dinh CV, Prather KJ. Dynamic control of metabolism. *Annu. Rev. Chem. Biomol. Eng.* **2021**, *12*, 519–541.
7. Li Z, Gao C, Ye C, Guo L, Liu J, Chen X, et al. Systems engineering of *Escherichia coli* for high-level shikimate production. *Metab. Eng.* **2023**, *75*, 1–11.
8. Ge C, Sheng H, Chen X, Shen X, Sun X, Yan Y, et al. Quorum sensing system used as a tool in metabolic engineering. *Biotechnol. J.* **2020**, *15*, 1900360.
9. Chigozie VU, Saki M, Esimone CO. Molecular structural arrangement in quorum sensing and bacterial metabolic production. *World J. Microbiol. Biotechnol.* **2025**, *41*, 71.
10. Song J, Zhuang M, Du C, Hu X, Wang X. Metabolic engineering of *Escherichia coli* for self-induced production of L-isoleucine. *ACS Synth. Biol.* **2025**, *14*, 179–192.
11. Liu H. Autonomous production of 1,4-butanediol via a *de novo* biosynthesis pathway in engineered *Escherichia coli*. *Metab. Eng.* **2015**, *29*, 135–141.
12. Wu J, Bao M, Duan X, Zhou P, Chen C, Gao J, et al. Developing a pathway-independent and full-autonomous global resource allocation strategy to dynamically switching phenotypic states. *Nat. Commun.* **2020**, *11*, 5521.
13. Tan GY, Peng Y, Lu C, Bai L, Zhong JJ. Engineering validamycin production by tandem deletion of γ-butyrolactone receptor genes in *Streptomyces Hygroscopicus* 5008. *Metab. Eng.* **2015**, *28*, 74–81.
14. Song J, Zhuang M, Fang Y, Hu X, Wang X. Self-regulated efficient production of L-threonine via an artificial quorum sensing system in engineered *Escherichia coli*. *Microbiol. Res.* **2024**, *284*, 127720.
15. Gu F, Jiang W, Mu Y, Huang H, Su T, Luo Y, et al. Quorum sensing-based dual-function switch and its application in solving two key metabolic engineering problems. *ACS Synth. Biol.* **2020**, *9*, 209–217.
16. He X, Chen Y, Liang Q, Qi Q. Autoinduced AND gate controls metabolic pathway dynamically in response to microbial communities and cell physiological state. *ACS Synth. Biol.* **2017**, *6*, 463–470.
17. Doong SJ, Gupta A, Prather KLJ. Layered dynamic regulation for improving metabolic pathway productivity in *Escherichia coli*. *Proc. Natl. Acad. Sci. USA* **2018**, *115*, 2964–2969.
18. Balagaddé FK, Song H, Ozaki J, Collins CH, Barnet M, Arnold FH, et al. A synthetic *Escherichia coli* predator-prey ecosystem. *Mol. Syst. Biol.* **2008**, *4*, 187.
19. Honjo H, Iwasaki K, Soma Y, Tsuruno K, Hamada H, Hanai T. Synthetic Microbial consortium with specific roles designated by genetic circuits for cooperative chemical production. *Metab. Eng.* **2019**, *55*, 268–275.
20. Cao Z, Liu Z, Mao X. Application of quorum sensing in metabolic engineering. *J. Agric. Food Chem.* **2023**, *71*, 5062–5074.
21. Kim E-M, Woo HM, Tian T, Yilmaz S, Javidpour P, Keasling JD, et al. Autonomous control of metabolic state by a quorum sensing (QS)-mediated regulator for bisabolene production in engineered *E. coli*. *Metab. Eng.* **2017**, *44*, 325–336.
22. Boo A, Ledesma Amaro R, Stan G-B. Quorum sensing in synthetic biology: a review. *Curr. Opin. Syst. Biol.* **2021**, *28*, 100378.
23. Ge C, Yu Z, Sheng H, Shen X, Sun X, Zhang Y, et al. Redesigning regulatory components of quorum-sensing system for diverse metabolic control. *Nat. Commun.* **2022**, *13*, 2182.
24. Shong J, Huang Y-M, Bystroff C, Collins CH. Directed evolution of the quorum-sensing regulator EsaR for increased signal sensitivity. *ACS Chem. Biol.* **2013**, *8*, 789–795.
25. Li J, Liu R, Chen Y, Liu S, Chen C, Liu T, et al. Computer-aided rational engineering of signal sensitivity of quorum sensing protein LuxR in a whole-cell biosensor. *Front. Mol. Biosci.* **2021**, *8*, 729350.
26. Bao S-H, Li W-Y, Liu C-J, Zhang D-Y, Meng E. Quorum-sensing based small RNA regulation for dynamic and tuneable gene expression. *Biotechnol. Lett.* **2019**, *41*, 1147–1154.
27. Miller GL. Use of dinitrosalicylic acid reagent for determination of reducing sugar. *Anal. Chem.* **1959**, *31*, 426–428.
28. Önal A. A review: Current analytical methods for the determination of biogenic amines in foods. *Food Chem.* **2007**, *103*, 1475–1486.
29. Kumar L, Patel SKS, Kharga K, Kumar R, Kumar P, Pandohee J, et al. Molecular mechanisms and applications of *N*-acyl homoserine lactone-mediated quorum sensing in bacteria. *Molecules* **2022**, *27*, 7584.
30. Yu Z, Yu D, Mao Y, Zhang M, Ding M, Zhang J, et al. Identification and characterization of a LuxI/R-type quorum sensing system in *Pseudoalteromonas*. *Res. Microbio.* **2019**, *170*, 243–255.
31. Wang Y, Bian Z, Wang Y. Biofilm formation and inhibition mediated by bacterial quorum sensing. *Appl. Microbiol. Biotechnol.* **2022**, *106*, 6365–6381.
32. Haseltine EL, Arnold FH. Implications of rewiring bacterial quorum sensing. *Appl. Environ. Microbiol.* **2008**, *74*, 437–445.
33. Gupta A, Reizman IMB, Reisch CR, Prather KLJ. Dynamic regulation of metabolic flux in engineered bacteria using a pathway-independent quorum-sensing circuit. *Nat. Biotechnol.* **2017**, *35*, 273–279.

34. Cao H, Villatoro-Hernandez J, Weme RDO, Frenzel E, Kuipers OP. Boosting heterologous protein production yield by adjusting global nitrogen and carbon metabolic regulatory networks in *Bacillus subtilis*. *Metab. Eng.* **2018**, *49*, 143–152.
35. Hanzelka BL, Greenberg EP. Evidence that the N-terminal region of the *Vibrio fischeri* LuxR protein constitutes an autoinducer-binding domain. *J. Bacteriol.* **1995**, *177*, 815–817.
36. Shadel GS, Young R, Baldwin TO. Use of regulated cell lysis in a lethal genetic selection in *Escherichia coli*: Identification of the autoinducer-binding region of the LuxR protein from *Vibrio fischeri* ATCC 7744. *J. Bacteriol.* **1990**, *172*, 3980–3987.
37. Slock J, VanRiet D, Kolibachuk D, Greenberg EP. Critical regions of the *Vibrio fischeri* LuxR protein defined by mutational analysis. *J. Bacteriol.* **1990**, *172*, 3974–3979.
38. Segobia DJ, Trasarti AF, Apesteguía CR. Impact of solvent on Co/SiO_2 activity and selectivity for the synthesis of n-butylamine from butyronitrile hydrogenation. *Catal. Commun.* **2015**, *62*, 62–66.
39. Kim DI, Chae TU, Kim HU, Jang WD, Lee SY. Microbial production of multiple short-chain primary amines via retrobiosynthesis. *Nat. Commun.* **2021**, *12*, 173.
40. Park JH, Lee KH, Kim TY, Lee SY. Metabolic engineering of *Escherichia coli* for the production of L-valine based on transcriptome analysis and in silico gene knockout simulation. *Proc. Natl. Acad. Sci. USA* **2007**, *104*, 7797–7802.
41. Gao H, Tuyishime P, Zhang X, Yang T, Xu M, Rao Z. Engineering of microbial cells for L-valine production: challenges and opportunities. *Microb. Cell Fact.* **2021**, *20*, 172.
42. Yang Y-T, Bennett GN, San K-Y. The effects of feed and intracellular pyruvate levels on the redistribution of metabolic fluxes in *Escherichia coli. Metab. Eng.* **2001**, *3*, 115–123.
43. Wang J. Developing a pyruvate-driven metabolic scenario for growth-coupled microbial production. *Metab. Eng.* **2019**, *55*, 191–200.
44. Kimura Y, Tashiro Y, Saito K, Kawai-Noma S, Umeno D. Directed evolution of *Vibrio fischeri* LuxR signal sensitivity. *J. Biosci. Bioeng.* **2016**, *122*, 533–538.
45. Tashiro Y, Kimura Y, Furubayashi M, Tanaka A, Terakubo K, Saito K, et al. Directed evolution of the autoinducer selectivity of *Vibrio fischeri* LuxR. *J. Gen. Appl. Microbiol.* **2016**, *62*, 240–247.
46. Fernández-Cabezón L, Rosich i Bosch B, Kozaeva E, Gurdo N, Nikel PI. Dynamic flux regulation for high-titer anthranilate production by plasmid-free, conditionally-auxotrophic strains of *Pseudomonas Putida*. *Metab. Eng.* **2022**, *73*, 11–25.
47. Cao Z, Liu Z, Zhang G, Mao X. P mutants with different promoting period and their application for quorum sensing regulated protein expression. *Food Sci. Hum. Wellness* **2023**, *12*, 1841–1849.
48. Ding N, Zhou S, Deng Y. Transcription-factor-based biosensor engineering for applications in synthetic biology. *ACS Synth. Biol.* **2021**, *10*, 911–922.
49. Xu X, Li X, Liu Y, Zhu Y, Li J, Du G, et al. Pyruvate-responsive genetic circuits for dynamic control of central metabolism. *Nat. Chem. Biol*. **2020**, *16*, 1261–1268.
50. Xu P, Li L, Zhang F, Stephanopoulos G, Koffas M. Improving fatty acids production by engineering dynamic pathway regulation and metabolic control. *Proc. Natl. Acad. Sci. USA* **2014**, *111*, 11299–11304.
51. Wachsmuth M, Findeiss S, Weissheimer N, Stadler PF, Morl M. *De novo* design of a synthetic riboswitch that regulates transcription termination. *Nucleic Acids Res.* **2013**, *41*, 2541–2551.
52. Zhou L, Ren J, Li Z, Nie J, Wang C, Zeng A-P. Characterization and engineering of a clostridium glycine riboswitch and its use to control a novel metabolic pathway for 5-aminolevulinic acid production in *Escherichia coli*. *ACS Synth. Biol.* **2019**, *8*, 2327–2335.
53. Harder B, Bettenbrock K, Klamt S. Temperature-dependent dynamic control of the TCA cycle increases volumetric productivity of itaconic acid production by *Escherichia coli*. *Biotechnol. Bioeng.* **2018**, *115*, 156–164.
54. Yin X, Shin H-D, Li J, Du G, Liu L, Chen J. P_{gas}, a low-pH-induced promoter, as a tool for dynamic control of gene expression for metabolic engineering of *Aspergillus niger*. *Appl. Environ. Microbiol.* **2017**, *83*, e03222-16.
55. Hwang HJ, Kim JW, Ju SY, Park JH, Lee PC. Application of an oxygen-inducible *Nar* promoter system in metabolic engineering for production of biochemicals in *Escherichia coli*. *Biotechol. Bioeng.* **2017**, *114*, 468–473.
56. Hartline CJ, Schmitz AC, Han Y, Zhang F. Dynamic control in metabolic engineering: theories, tools, and applications. *Metab. Eng.* **2021**, *63*, 126–140.
57. Hao Y, Pan X, You J, Li G, Xu M, Rao Z. Microbial production of branched chain amino acids: advances and perspectives. *Bioresour. Technol.* **2024**, *397*, 130502.
58. Luo Q, Ding N, Liu Y, Zhang H, Fang Y, Yin L. Metabolic engineering of microorganisms to produce pyruvate and derived compounds. *Molecules* **2023**, *28*, 1418.
59. Blombach B, Schreiner ME, Holátko J, Bartek T, Oldiges M, Eikmanns BJ. L-valine production with pyruvate dehydrogenase complex-deficient *Corynebacterium glutamicum*. *Appl. Environ. MicrobioL.* **2007**, *73*, 2079–2084.
60. Cai M, Zhao Z, Li X, Xu Y, Xu M, Rao Z. Development of a nonauxotrophic L-homoserine hyperproducer in *Escherichia coli* by systems metabolic engineering. *Metab. Eng.* **2022**, *73*, 270–279.
61. Liu M, Cao Z. Regulation of NADH oxidase expression via a thermo-regulated genetic switch for pyruvate production in *Escherichia coli*. *Biotechnol. Bioproc. E.* **2018**, *23*, 93–99.